Real-Time Quantitative Imaging of Failure Events in Materials under Load at Temperatures above 1700°C

Hrishikesh A. Bale[1], Abdel Haboub[2], Alastair A. MacDowell[2], James R. Nasiatka[2], Dilworth L. Parkinson[2], Brian N. Cox[3], David B. Marshall[3] and Robert O. Ritchie[1,2*]

Ceramic-matrix composites are the emerging material of choice for structures that will see temperatures above ~1500°C in hostile environments, e.g., for next-generation gas turbines and hypersonic-flight applications. Technology has overcome the inherent brittleness of ceramics by creating hybrid-microstructures, made for example by fiber weaving. As in natural tissues (bone, seashells), tailored microstructural complexity imparts mechanical toughness, essential to avoiding failures. However, these materials are not easily analyzed to assess structural integrity; safe operation depends on how small cracks forming inside the material are restrained by its microstructure. Key to predicting safe life is gathering explicit 3-D observations of damage evolution in extreme environments, a previously unsolved experimental challenge. We report the observation of fully-resolved sequences of microcrack damage, imaged using synchrotron x-ray computed micro-tomography, as cracks grow under load at temperatures up to 1750°C. Such 3-D observations are key ingredients for high-fidelity simulations used to compute failure risks under extreme operating conditions.

[1] Department of Materials Science and Engineering, University of California, Berkeley, CA.
[2] Lawrence Berkeley National Laboratory, Berkeley, CA.
[3] Teledyne Scientific Company, Thousand Oaks, CA.
[*] To whom correspondence should be addressed. Email: roritchie@lbl.gov.

X-ray computed micro-tomography (μ-CT), using the high fluxes from synchrotron sources, has evolved into a powerful imaging tool in the fields of physical and biological sciences from its ability to image structure *in three-dimensions* (3-D) with high spatial resolution at macroscopic to sub-microscopic scales (*1,2*). With the development of increasingly complex structural materials, such as fiber-reinforced ceramic composites and polymer-matrix composites that are finding increasing use in cutting-edge aerospace applications (*3-7*), 3-D characterization of both structure and damage processes is essential, for it is the geometry, scale and nature of these structures in all three dimensions that control their properties.

The last decade has witnessed the emergence of strong and tough ceramic-matrix composites, within which various design strategies are used on different spatial scales to overcome the brittleness that is inherent in materials that are able to survive extreme temperatures and chemically corrosive environments. Strong continuous fiber bundles (scale 0.1–1 mm) are woven in custom-designed 3-D patterns, with individual bundles oriented in space so that they will follow the primary load paths expected in a given component to maximize its strength, and interlocked with one another to prevent catastrophic separation when damaged *(3).* Larger interstices between the fiber bundles may be partially filled with randomly-oriented fine reinforcing rods (scale: 1–10 μm), inhibiting local cracking under thermal shock. Coatings applied to individual fibers (scale: 0.1–1 μm) inhibit chemical reactions and ensure that the interfaces between the

fibers and the matrix remain weak, allowing a ductile response through matrix cracking and frictional pullout of crack-bridging fibers. The remaining space between coated fibers, fiber bundles, and reinforcing rods is filled with a ceramic-matrix material, which itself may be a hybrid containing, for example, graphitic sheets that inhibit oxygen ingress (scale: 1–100 nm) (*8*). Thus, like many natural materials, these new ceramic composites achieve robustness through complexity: their hierarchical, hybrid microstructure impedes the growth of local damage and prevents the large fatal cracks that are characteristic of brittle materials.

However, complexity in composition brings complexity in safe use. Most engineering structures, airframes, ships, buildings, etc., are designed to tolerate quite large cracks, which can be safely left monitored but unattended if they are less than a critical length, e.g., 10 mm or more in an airframe. Such cracks are large compared to the internal microstructural heterogeneity of a conventional material, which makes the prediction of their growth relatively easy; the effects of heterogeneity on crack growth tend to average out and therefore need not be included explicitly in engineering safety codes (*9*). For ceramic composites in ultrahigh-temperature applications, especially where corrosive species in the environment must be kept out of the material, relatively small cracks, on the order of the thickness of a fiber bundle (~1 mm), can be unacceptable. These new ceramic materials thus violate the simplifying maxim of most traditional

materials, that they be considered homogeneous on the scale at which damage becomes critical.

Exactly how micro-cracks are restrained by such tailored microstructure becomes the central question for the materials scientist who seeks to find the optimal composition or architecture and the design engineer who must predict the failure envelope. These questions raise many challenges: the conditions of interest are extreme. Observational methods based on direct imaging of the surface are complicated by high thermal noise (but see a recent breakthrough in optical digital-image correlation performed at 1500°C (*10*)). The properties (strength, etc.) of the composite's constituent materials and their interfaces are generally unknown at high temperature; they are also impossible to calibrate by independent tests, because the strength of different phases combined at nm and μm scales is not represented by tests on large specimens of the phase isolated as a monolithic material.

Measurements made at high temperature are the only faithful source of the details of failure. If a test specimen is cooled to an experimentally convenient 25°C for examination, the very act of cooling introduces thermal strains, of the order of at least 0.1–0.5% depending on composition and cooling rate, which can completely change the cracking patterns present before such cracks can be measured. *In situ* tomographic observations of deformation in an aluminum alloy have been made at temperatures as

high as 555°C by Terzi et al (11). However, this temperature is much lower than the range of interest for ceramic composites.

In this work, we describe research to enable the mechanical and 3-D structural characterization of ceramic composites *in situ*, i.e., under load at ultrahigh temperatures.

In situ x-ray μ-CT imaging at ultrahigh-temperature under load

We have developed a unique facility that permits real-time μ-CT under tensile or compressive loads at very high temperatures for the 3-D imaging of materials using synchrotron x-rays. The notable features of the set-up are the ability to maintain an *in situ* temperature environment of up to 1750°C in inert or oxidizing atmospheres with a controlled load applied to the sample, while simultaneously imaging in real time with x-rays. The system is capable of generating 3-D tomograms at a sufficiently high spatial resolution of 0.65 μm/voxel to image structural details at the micro-scale and to resolve the opening displacements of internal microcracks and other forms of internal damage as a function of load.

Schematics of the *in situ* rig and its working principles are shown in Fig. 1. Detailed procedures are given in the *Methods* section with further information available in the Supplementary information online. The sample is held by water-cooled grips in the center of a vacuum-sealed cell of diameter ~170 mm, which can be evacuated and backfilled with a selected gas. Heating is provided by a hexapole arrangement of 150 watt halogen lamps, each with an ellipsoidal reflector aimed at the center of the cell (Fig

1b), giving a spherical hot zone of diameter ~5 mm. Temperatures of test samples in the hot zone were determined from separate calibration of lamp power with thermocouples (see Supplementary online information). The waist of the cell consists of a cylindrical aluminum window (300 μm thickness, 7 mm height), which allows x-rays to illuminate the sample and pass through to an x-ray imaging system (Fig.1c) consisting of a scintillator coupled with microscope optics to a digital camera (*12*). For each scan, a set of 1200 radiographs are collected and converted to a reconstructed 3-D tomographic image using inverse radon transforms.

Images formed with the coherent synchrotron x-ray source contain a mixture of phase and absorption contrast (*13*), which emphasizes edges and can make quantitative measurement of crack openings difficult. To minimize phase-contrast effects we used the Modified Bronnikov Algorithm (MBA) and filtered back-projection to obtain a 3-D tomographic reconstruction of the phase signal, enabling more accurate quantitative structural measurements (*14*).

Ceramic matrix composite materials for in situ observations

We chose to examine two SiC-based composites to illustrate the capability for 3-D imaging under load at ultrahigh temperatures and the potential for revealing microscopic damage mechanisms that control strength and toughness. These materials were selected because of their exceptional combination of strength-to-weight ratio and

high-temperature capability, which make them the most important candidate materials for future structural and engine applications at extreme temperatures.

One composite was in the form of rods (~1 mm diameter, 55mm length) consisting of a single tow of SiC fibers (Nippon Carbon Hi-Nicalon Type-S, 500 fibers/tow, fiber diameter 10 μm) embedded within a matrix of SiC formed by chemical-vapor infiltration (CVI). The other was in the shape of beams (~2x3x55 mm) cut from a plate of textile-based composite consisting of a woven preform of carbon fiber tows (angle interlock weave structure, T300 carbon fibers, 6,000 fibers/tow, fiber diameter 7 μm) embedded in a matrix of SiC formed by a combination of CVI and infiltration/pyrolysis of a slurry of SiC particles in a polymer precursor for SiC (*15*). The fibers within each composite were surrounded by thin weak interphases of thickness ~0.5–2 μm; boron nitride in SiC_f-SiC_m and pyrolytic carbon in C_f-SiC_m. Additional details on these materials are given in the *Methods* section.

Test specimens, with 15 mm gauge length, were bonded, using high-temperature material similar to the matrix of the C_f-SiC_m composite, into threaded molybdenum grips (*16*), which were then mounted in a self-aligning ball-and-socket loading fixture in the test chamber. Tomography data for each specimen were collected while tensile forces were applied in steps by a displacement-controlled loading system, increasing monotonically from 10 N until the peak load carrying capacity was exceeded (Figs. 2-4). Each image consists of several tiled scans to increase the field of view. After each load

step, an initial small load relaxation (< 5%) was observed, followed by a period of constant load for the duration of the image acquisition (~20 minutes for each scan plus additional time for mechanical stabilization after moving the stage, giving a total period up to 90 minutes for 3 tiled scans). The absence of load relaxation during image acquisition at high temperature indicated that deformation due to time-dependent mechanisms such as creep were negligible in these experiments.

Observation of damage evolution under combined load and temperature

The single-tow specimens were imaged with magnification corresponding to 0.65 μm/voxel over a 5 mm length of test section, in tests carried out at both ambient and 1750°C. The individual fibers and BN coatings are readily resolved in cross-sectional slices normal to the fiber tows (Fig. 2a) with no discernible difference in resolution between low- and high-temperature images. At both temperatures, cracks developed in the matrix during loading, which from the 3-D images can be seen to extend continuously in the matrix through the cross-section of the composite, while the entire load was carried by intact fibers bridging these cracks. In these and other tests, the paths of the matrix cracks showed some variability. Most were close to a single planar surface normal to the applied load. However, some followed a helical path around the fiber axis, with ends joined by a crack segment parallel to the axis (top crack in Fig. 3), similar to earlier μ-CT observations in room-temperature tests on similar composite specimens (*17*), while others were branched, as in the high-temperature specimen in

Fig. 2. Beginning at ~100 N tensile load (below peak load), broken fibers were detected at locations distributed throughout the volume of the composite. The number of broken fibers increased with increasing load, with up to 20% of the fibers breaking before peak load. Eventually, the fibers pulled out completely from the matrix (Fig. 2). The 3-D images reveal a wealth of information on the events occurring in the interior of the composite during this failure process: the loads and locations at which individual fibers broke, the distances the fibers relaxed after breaking, the opening displacements of the matrix cracks, and the 3-D surfaces of the matrix cracks. This can be seen in Fig. 3; further details are given in the movie files S1 and S2 in the Supplementary online information corresponding, respectively, to the ambient and high temperature experiments.

The occurrence of crack bridging, which is essential to toughening these materials, is enabled by the weak BN interphase, which allows debonding and sliding between the fibers and matrix. The magnitude of the sliding resistance dictates how multiple cracks form in the matrix (*18*), which in turn dictates the macroscopic stress-strain response of the composite. Specifically, the friction stress determines a limiting lower-bound for the applied tensile stress at which matrix cracking can occur (*19-21*) (which relates to the onset of inelastic deformation), as well as a characteristic length over which sliding occurs and stress is transferred between the fibers and the matrix. The sliding distance determines the spacing and the opening displacements of matrix cracks as well as the

relaxation of fibers that are broken within the matrix. The crack spacing and opening displacements are responsible for the nonlinear stress-strain response after the onset of inelastic behavior.

Quantitative analysis of μ-CT data

While the tomography images confirm similarity in the toughening mechanism at 25°C and at 1750°C, they also reveal differences that indicate a change in the sliding resistance at high temperature:

(i) At a given load, the matrix crack-opening displacement was larger at 1750°C than at 25°C (Fig. 2). As long as the sliding zones associated with adjacent cracks do not overlap and a significant number of fibers are not broken, the magnitude of the frictional stress can be calculated from the crack-opening displacements. From the images obtained at 127 N load (Fig. 2), we obtain frictional stresses of 2 MPa for the room-temperature test, (crack opening 16 μm) and 0.4 MPa for the high-temperature test (crack opening 75 μm). Details of this calculation are given in the Supplemental information. From these values of frictional stress we calculate sliding lengths (and thus crack spacings) of ~3 mm at 25°C and ~13 mm at 1750°C.

(ii) At 25°C, multiple matrix cracks (three) formed within the test section at loads between the imaging steps at 113 N and 127 N, whereas at 1750°C a single crack formed at 45 N load (Fig. 2). In both cases, the crack-opening displacements continued to increase with further loading, while no new cracks were formed (confirmed also by

scanning electron microscope (SEM) observations after loading to failure). The room-temperature results are consistent with observations from separate *ex situ* tests using samples with longer test sections (60 mm), which showed a distribution of cracks separated by distances between 1 and 4 mm (average 2 mm), which is consistent with calculated sliding lengths (above). In the high-temperature specimen, the observation of a single crack is also consistent with the calculated sliding length, which in this case exceeds half the gauge length.

(iii) Differences were seen in the statistical distributions of fiber failure sites and relaxation lengths at 25°C and 1750°C (seen in Fig. 3 and movie files S1 and S2). At high temperature, failure sites were distributed over larger distances from the matrix cracks and the relaxation distances were larger than at 25°C. These observations are also consistent with the sliding resistance being smaller at 1750°C than at 25°C. The distributed loads and positions of fiber fractures relate directly to the statistical distribution of fiber strengths (*22*,*23*) (if the fiber strengths were single-valued, all failures would occur at the plane of the matrix crack) and can be used to evaluate the parameters characterizing this distribution. There is currently no other way to access this information, which is critical for detecting and quantifying changes in fiber properties due to high-temperature heat treatments and possible chemical reactions during processing of the composite.

These results from *in situ* tomography provide new insight into how the 3-D behavior in SiC_f-SiC_m composites under tensile load differs at 25°C and at 1750°C. The observed reduction in fiber sliding resistance at high temperature could potentially be caused by changes in residual stresses due to thermal expansion mismatch. However, residual stresses in this composite are expected to be small. Another possible mechanism is a change in the shear properties of the boron nitride layer between the fibers and matrix at high temperature.

Results obtained from similar loading experiments using C_f-SiC_m textile composite specimens, with a larger length-scale and more complex architecture than the single-tow samples, are shown in Fig. 4A–C (Detailed views of cracks initiating and propagating in the room and high temperature specimens are shown, respectively, in the movie files S3 and S4 in the Supplemental online information). Once more, differences can be seen in the development of cracks at 25°C and 1750°C. Images here were recorded at lower resolution (1.3 μm/voxel) to allow a larger field of view. The individual carbon fibers in this composite were not visible in the sections normal or parallel to the fiber tows, because of this lower resolution and the minimal density difference between the fibers and the pyrolytic-carbon coatings. Nevertheless, the fiber tows are clearly distinguished from the denser matrix, which consists of two layers; one a thin brighter layer of CVI SiC surrounding all of the fiber tows and the other the polymer-derived SiC filling the remaining space. Images obtained at 25°C and 1750°C

were of identical quality. During initial loading at both temperatures, cracks formed in the matrix normal to the loading direction at positions where the matrix lay over a transverse fiber tow. With increasing load, the cracks grew through the transverse tows until they met an underlying axial tow (at loads in the range ~40 N to 70 N), where they were deflected. At 25°C this deflection involved formation of multiple splitting cracks (Fig. 4), which progressed incrementally along the centers of the axial tows as the load was increased to the peak value of 150 N. At 1750°C, the deflection of the crack at each tow involved a single crack that grew along the edge of the axial fiber tows as the load increased to 120 N, whereupon there was a large load drop. By influencing the access of ambient gas to the internal reinforcing fibers, differences in crack paths such as these could potentially have a large effect on subsequent high-temperature oxidation damage. Further experiments are needed to determine the reason for the difference in crack paths and to assess whether similar differences in cracking behavior are consistently observed in other loading directions.

Summary

In this exploratory study only a small fraction of the quantitative and statistical information potentially available in the μ-CT data sets was used. The μ-CT data contain complete quantitative information on crack paths, crack surface areas and orientations, spatial variations in the crack-opening displacements, statistics of relative spatial location of cracks and microstructural heterogeneities within the sample volume; all

these parameters are critical in any analysis of fracture as they govern the toughness of the material. The challenge is to extract this information from the reconstructed 3-D images in a form that can be readily used for validation of computational models and to provide calibration of material constitutive laws as input for the models. Success rests on efficient methods for processing the 3-D image data with techniques such as segmentation for automated identification and representation of cracks and microstructural features. The images in Fig. 3 (and the movie files S1 and S2) are examples of such representations obtained from the image data in Fig. 2 through the use of multiple image post-processing steps (see Supplemental information).

We have demonstrated that *in situ* x-ray micro-tomography can now be used for studying advanced materials that are being designed for future ultrahigh temperature environments. The means to acquire real-time high-resolution (up to 0.65 μm/voxel) 3-D structural data for ceramic-matrix composites has been presented with the ability to observe microstructure and damage under load at different hierarchical length-scales (from a micrometer to several millimeters) at unprecedented temperatures as high as 1750°C. The results contain vital information pertaining to the underlying failure mechanisms within ceramic composites that can be used to optimize their performance. An extension of this study would involve rigorous analysis and interpretations of the different physical phenomena occurring *in situ* under the complex environment of load and temperature. The study of time-dependent damage mechanisms involving high-

temperature creep would be facilitated by reducing the scan time for image acquisition. Scan times at the Advanced Light Source (ALS) facility, where this work was performed, have recently been reduced to several minutes without loss of image quality through use of a high frame rate camera and an improved high-efficiency scintillator. Even shorter scan times can be achieved at the expense of image quality by limiting the number of radiographs collected in each scan. These and other advances in synchrotron facilities show promise for enabling *in situ* tomography under near-continuous loading conditions. The capacity of validating the models developed for virtual testing through direct, real-time, non-invasive experimental observations will greatly advance our understanding and help promote the innovation of these technologically important materials.

Methods

Materials

The single-tow SiC_f-SiC_m composite specimens were fabricated at Hypertherm, Inc. (Huntington Beach, CA) by winding a SiC fiber tow on a carbon frame and processing by chemical-vapor infiltration in two steps, the first to deposit a thin layer of boron nitride that was doped with silicon to improve its oxidation resistance, and the second to deposit the matrix of SiC. The textile-based C_f-SiC_m composite was fabricated by first infiltrating a woven fabric of carbon fiber tows with a thin fiber coating of pyrolytic carbon followed by a thin layer of SiC by CVI (at Hypertherm, Inc.) then forming the remaining matrix by multiple cycles of infiltration and

pyrolysis of a slurry consisting of sub-micron particles of silicon carbide in a polymer (Allylhydridopolycarbosilane) that decomposes at high temperature to form SiC. The textile fabric was a three-layer angle-interlock structure, consisting of three layers of relatively straight weft fiber tows linked together with side-by-side warp fiber tows that follow almost sinusoidal paths through the thickness of the composite. The test samples were cut from a large plate with the warp fiber tows along the axial lengths of the beams.

μ-CT characterization

We used the hard X-ray beamline BL 8.3.2 at the Advanced Light Source (Lawrence Berkeley National Laboratory, CA) for the μ-CT tomography experiments. The ultrahigh-temperature tensile rig was mounted on an air bearing rotation stage that was positioned the beam by means of translation stages. In the case of the high-temperature experiments, a non-oxidizing environment is maintained by admitting a low flow of high purity nitrogen while pumping to 10^{-3} torr. Load is applied to the sample by a stepper motor, while force and displacement are measured using an in-line load cell and a linear variable differential transformer (LVDT) sensor. A 300 μm thick aluminum window allows tensile forces up to 2 kN to be applied to the test sample while obtaining x-ray transmission of ~90% with the filtered white light (2.5 mm aluminum filter) used for sample illumination at a sample-to-detector distance of 150 mm. Tomography data for each specimen were collected while tensile forces were applied in steps, increasing monotonically from 10 N until the peak load carrying capacity was exceeded. Each image consists of several tiled scans to increase the field of view.

For the smaller, single tow specimens, a magnification corresponding to 0.65 μm/voxel was used, giving a vertical field of view of approximately 1.4 mm. The full 3-D dataset for this

sample consists of four adjacent scans "tiled" along the vertical direction, covering over 5.5 mm of the sample; for the textile composite specimen the data were collected in two vertical tiles with a magnification corresponding to 1.3 μm/voxel, covering nearly 5 mm total of the specimen. Each scan consisted of multiple exposures, each of 100 ms, collected at 0.125° angular steps over a 180° rotation of the sample.

Tomographic slices were generated using a commercial reconstruction algorithm (Octopus v8; IIC UGent, Zwijnaarde, Belgium). Data were processed using image processing tools in ImageJ (Rasband, W.S., ImageJ, U. S. National Institutes of Health, Bethesda, Maryland, USA, http://imagej.nih.gov/ij/, 1997-2011.) and visualized in Avizo 6.1 (VSG, Visualization Sciences Group, Inc., Burlington, MA). For crack segmentation, the wavelet-FFT algorithm (referred to as xStripes) developed by Muench et al. (*24*) was adapted for use in ImageJ. Transverse μ-CT slices parallel to the axis of the fibers produced striped patterns of the fibers which are eliminated by the wavelet-FFT filter. Filtered slices contained grayscale information of cracks alone, which were binarized and further segmented to obtain the crack-opening measurements. The magnitudes of the frictional sliding stresses were calculated from the crack-opening displacements using the following expression the approach of Marshall, Cox and Evans (*20*); details are given in the Supplementary online information.

Temperature measurement

Measurement of high temperatures in this test setup is challenging as the small size of the test samples precludes directly attaching or embedding thermocouples. In these experiments, the sample temperatures in the hot zone were estimated from separate calibration tests, in which a C-type tungsten-rhenium thermocouple (maximum measureable temperature of 2300°C) was

mounted into the top grips and translated across the field of view using the motorized loading stage, with x-ray transmission images being used to determine the thermocouple position. The variation within the central 5 mm of the field of view is approximately 150˚C at the set temperature of 1750°C. The operating temperature range of the furnace can be adjusted for a particular sample using calibrated voltage and current settings.

Further information on temperature measurements can be found in the Supplementary online information.

References and notes

1. Stock, S. R. Recent advances in x-ray microtomography applied to materials. *Int. Mater. Rev.* **53**, 129-181 (2008).

2. Sakdinawat, A. & Attwood, D. Nanoscale x-ray imaging. *Nat Photonics* **4**, 840-848 (2010).

3. Marshall, D. B. & Cox, B. N. Integral textile ceramic structures. *Annu. Rev. Mater. Res.*. **38**, 425-443 (2008).

4. Schmidt, S. *et al.* Ceramic matrix composites: A challenge in space-propulsion technology applications. *Int. J. Appl. Ceram. Tec.* **2**, 85-96 (2005).

5. Mouritz, A. P., Bannister, M. K., Falzon, P. J. & Leong, K. H. Review of applications for advanced three-dimensional fibre textile composites. *Compos. Part A-Appl.* S **30**, 1445-1461 (1999).

6. Morscher, G. N. & Pujar, V. V. Design guidelines for in-plane mechanical properties of sic fiber-reinforced melt-infiltrated SiC composites. *Int. J. Appl. Ceram. Tec.* **6**, 151-163 (2009).

7. Zhao, J. C. & Westbrook, J. H. Ultrahigh-temperature materials for jet engines. *MRS Bull.* **28**, 622-630 (2003).

8. Raj, R., Scarmi, A. & Soraru, G. D. The role of carbon in unexpected visco(an)elastic behavior of amorphous silicon oxycarbide above 1273k. *J. Non-Cryst. Solids* **351**, 2238-2243 (2005).

9. Zhuang, W., Barter, S. & Molent, L. Flight-by-flight fatigue crack growth life assessment. *Int. J. Fatigue* **29**, 1647-1657 (2007).

10. Novak, M. D. & Zok, F. W. High-temperature materials testing with full-field strain measurement: Experimental design and practice. *Rev. Sci. Instrum.* **82** (2011).

11. Terzi, S. et al. In situ x-ray tomography observation of inhomogeneous deformation in semi-solid aluminium alloys. *Scripta Mater.* **61**, 449-452 (2009).

12. Kinney, J. H. & Nichols, M. C. X-ray tomographic microscopy (xtm) using synchrotron radiation. *Annu. Rev. Mater. Sci.* **22**, 121-152 (1992).

13. Langer, M., Cloetens, P., Guigay, J.-P. & Peyrin, F. Quantitative comparison of direct phase retrieval algorithms in in-line phase tomography. *Med. Phys.* **35**, 4556-4566 (2008).

14. Groso, A., Abela, R. & Stampanoni, M. Implementation of a fast method for high resolution phase contrast tomography. *Opt. Express* **14**, 8103-8110 (2006).

15. Berbon, Z., Rugg, K. L., Dadkhah, M. S. & Marshall, D. B. Effect of weave architecture on tensile properties and local strain heterogeneity in thin-sheet C-SiC composites. *J. Am. Ceram. Soc.* **85**, 2039-2048 (2002).

16. Molybdenum was selected because its thermal expansion coefficient is similar to that of SiC over the temperature range 25°-1750°C.

17. Chateau, C. *et al.* In situ x-ray microtomography characterization of damage in SiC_f/SiC minicomposites. *Compos. Sci.Technol.* **71**, 916-924 (2011).

18. Budiansky, B., Evans, A. G. & Hutchinson, J. W. Fiber-matrix debonding effects on cracking in aligned fiber ceramic composites. *Int. J. Solids Struct.* **32**, 315-328 (1995).

19. Morscher, G. N. Tensile stress rupture of sicf/sicm minicomposites with carbon and boron nitride interphases at elevated temperatures in air. *J. Am. Ceram. Soc.* **80**, 2029-2042 (1997).

20. Marshall, D. B., Cox, B. N. & Evans, A. G. The mechanics of matrix cracking in brittle-matrix fiber composites. *Acta Metall. Mater.* **33**, 2013-2021 (1985).

21. Morscher, G. N., MartinezFernandez, J. & Purdy, M. J. Determination of interfacial properties using a single-fiber microcomposite test. *J. Am. Ceram. Soc.* **79**, 1083-1091 (1996).

22. Okabe, T., Nishikawa, M. & Curtin, W. A. Estimation of statistical strength distribution of carborundum polycrystalline SiC fiber using the single fiber composite with consideration of the matrix hardening. *Compos. Sci.Technol.* **68**, 3067-3072 (2008).

23. Cox, B. N., Marshall, D. B. & Thouless, M. D. Influence of statistical fiber strength distribution on matrix cracking in fiber composites. *Acta Metall. Mater.* **37**, 1933-1943 (1989).

24. Muench, B., Trtik, P., Marone, F. & Stampanoni, M. Stripe and ring artifact removal with combined wavelet - fourier filtering. *Opt. Express* **17**, 8567-8591 (2009).

Acknowledgements

Work supported by the Air Force Office of Scientific Research (Dr. Ali Sayir) and NASA (Dr. Anthony Calomino) under the National Hypersonics Science Center for Materials and Structures (AFOSR Contract No. FA9550-09-1-0477). We acknowledge the use of the x-ray synchrotron micro-tomography beam line (8.3.2) at the Advanced Light Source (ALS) at the Lawrence Berkeley National Laboratory, which is supported by the Office of Science of the U.S. Department of Energy under contract no. DE-AC02-05CH11231.

Author Contributions

B.N.C, D.B.M and R.O.R conceived the project, J.R.N and A.A.M. designed and built the equipment, D.B.M. prepared the composite samples, H.A.B. performed the experiments and analysis with assistance from A.H., A.A.M., D.L.P. and D.B.M., and H.A.B., B.N.C., D.B.M, and R.O.R. wrote the manuscript with contributions from A.A.M.

Additional information

The authors declare no competing interests. Supplementary information accompanies this paper. Correspondence and requests for materials should be addressed to R.O.R.

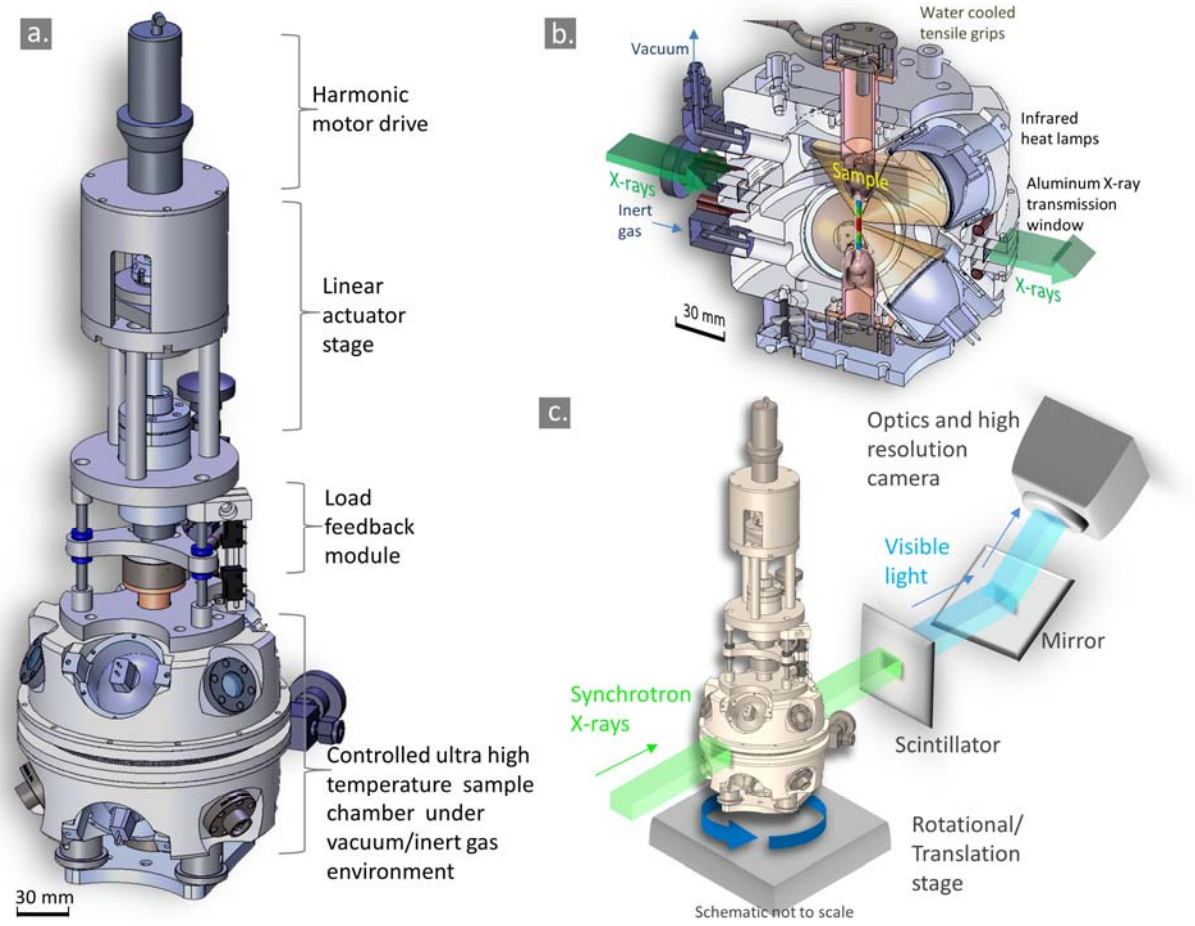

Figure 1. ***In Situ*** **Ultrahigh Temperature Tensile Test Rig**. (a) Schematic illustration of *in situ* ultrahigh temperature tensile test rig for synchrotron x-ray computed micro-tomography (Beamline 8.3.2 of Advanced Light Source, CA) (b) Sectional view of heating chamber illustrates x-ray transmission path through heating chamber and sample. We have used this chamber to test materials at temperatures as high as 1750°C. (c) Schematic of the rig in transmission mode for x-ray computed tomography.

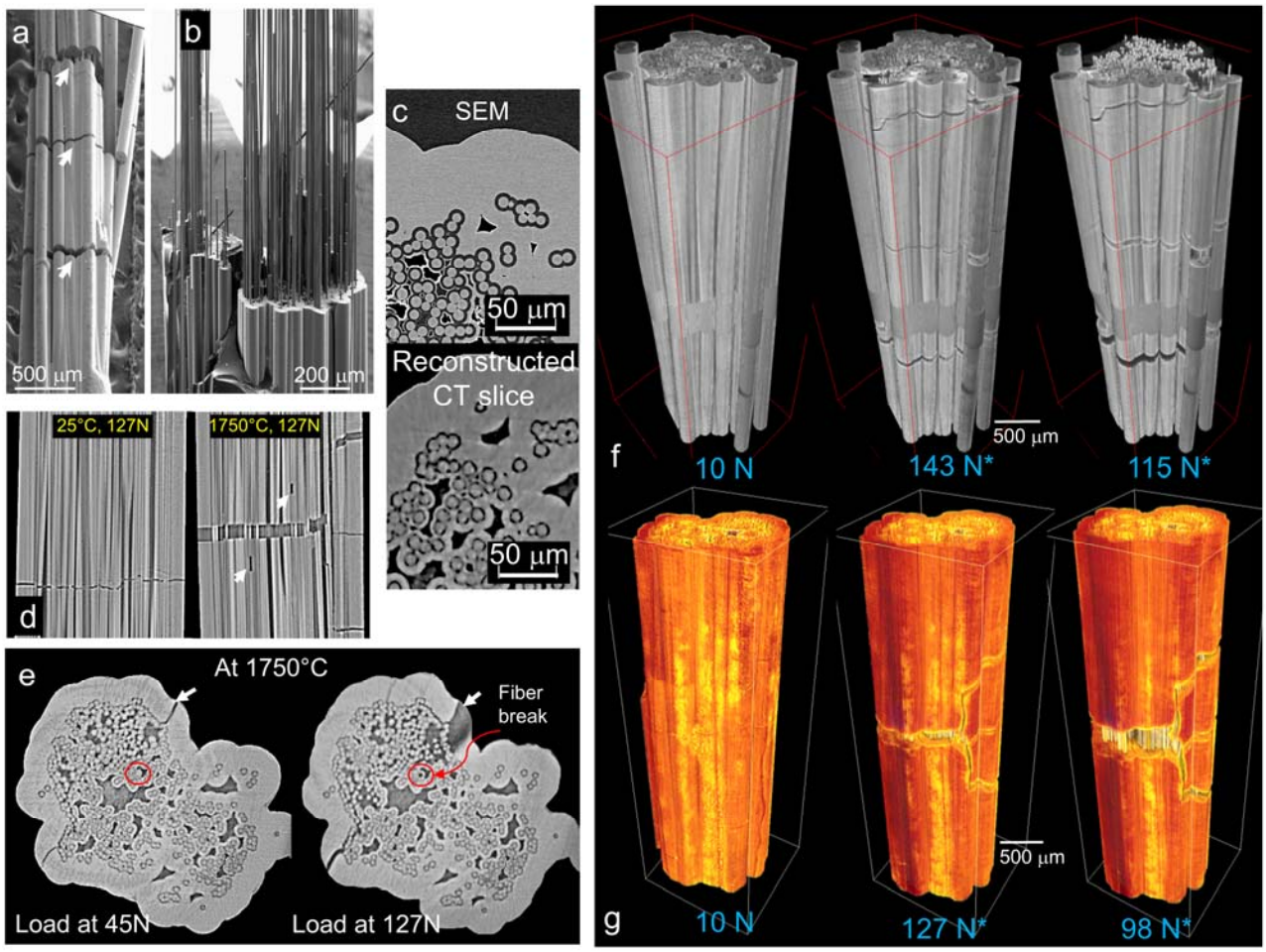

Figure 2. ***In situ*** **testing of single-tow SiC-SiC composite specimens at room (25°C) and ultrahigh (1750°C) temperatures.** Force-displacement curves are given in Fig. 3. (**a**) and (**b**) Scanning electron micrographs (SEM) of room-temperature specimen after testing. Arrows in (a) indicate multiple matrix cracks normal to applied tensile load. Image in (b) was taken after complete separation *ex situ*. Failure is associated with pullout of fibers from the matrix. (**c**) Comparison of image resolution in a reconstructed μ-CT slice from specimen in (a) before testing and a cross-sectional SEM image from another sample of the same composite. (**d**) Longitudinal μ-CT slices from tests at 25°C and 1750°C (both under applied load of 127 N), showing single planar crack in the former and bifurcated crack with two fiber breaks (indicated by arrows) in the latter. (**e**) Cross-section μ-CT slices from 1750°C specimen in (d) at two stages of loading (45N and 127N). Red circles indicate fiber that is intact at 45N and broken at 127N. (f) and (g) 3-D volume-rendered μ-CT images from specimens tested at room temperature (f) and at 1750°C (g) at several applied tensile loads as indicated (in Newtons). False colors were applied in (g) to highlight the different test temperatures.

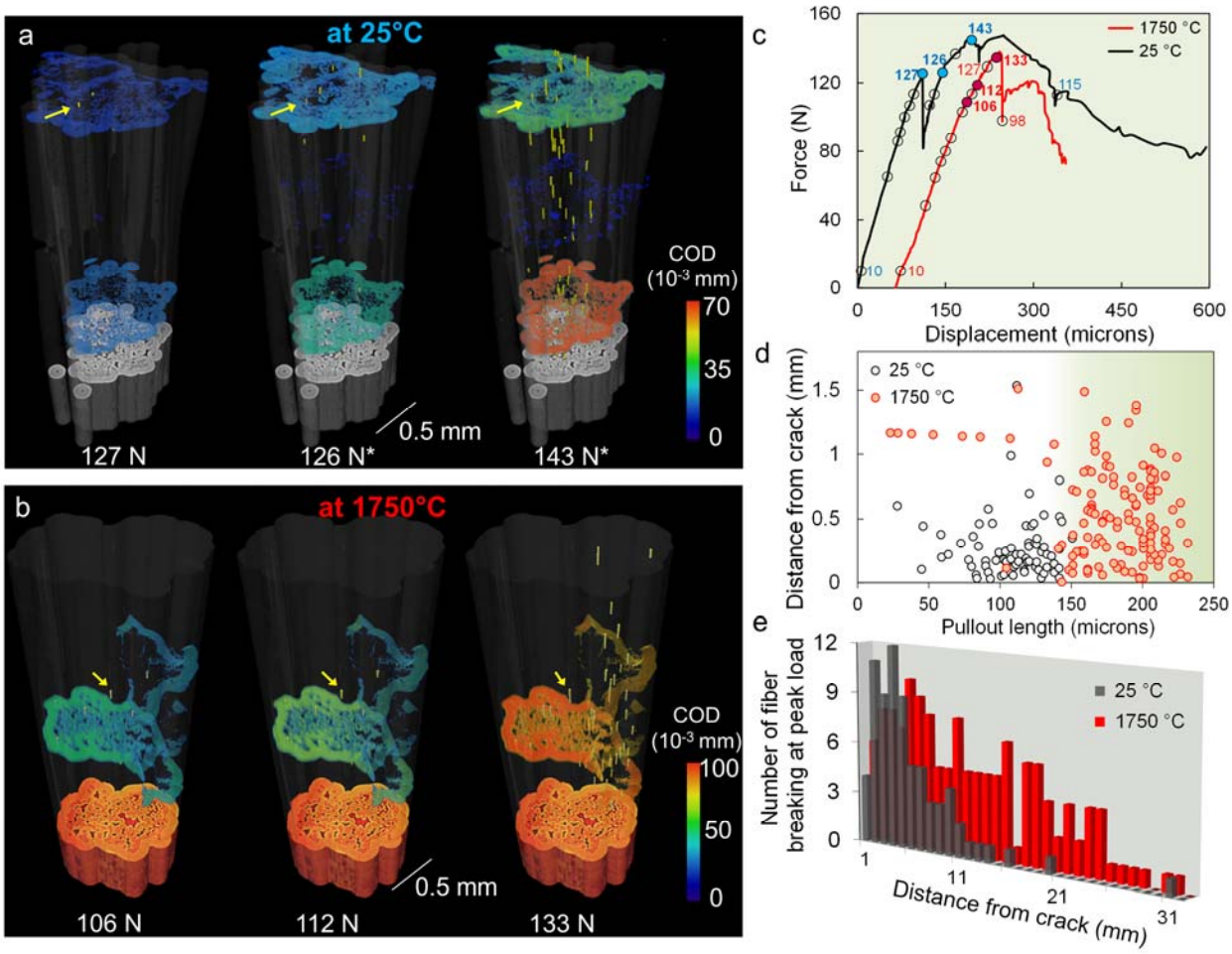

Figure 3. Quantification of cracks in matrix and fibers of single-tow SiC-SiC composite specimens from Fig. 2. (**a**) & (**b**) 3-D rendering from μ-CT data shows matrix cracks and individual fiber breaks in specimens tested at 25°C and 1750°C. The red-blue color scheme indicates opening displacements of matrix cracks, quantified by processing the 3-D tomography data. Yellow arrows indicate cylindrical holes remaining after relaxation of broken fibers. The fiber and matrix materials have been set transparent to reveal the cracks. (**c**) Force-displacement curves from *in situ* tests in (a) and (b). Red curve offset by 70 μm for visual clarity. Hollow circles indicate acquired μ-CT data at that load; blue and red solid circles indicate loads corresponding to images in (a) and (b) respectively. (**d**) Comparison of statistical data on fiber fracture at the peak loads in the specimens in (a) and (b): each symbol indicates the distance of a fiber fracture from the nearest matrix crack and the separation of the fractured fiber ends after relaxation by sliding; red circles correspond to 1750°C test, black circles to 25°C test. (**e**) Histograms of the number of broken fibers as a function of distance from the closest matrix cracks at peak load. Additionally detailed animations of the complete sets of μ-CT data from these two tests are included in the videos S1 and S2 in the Supplementary online information.

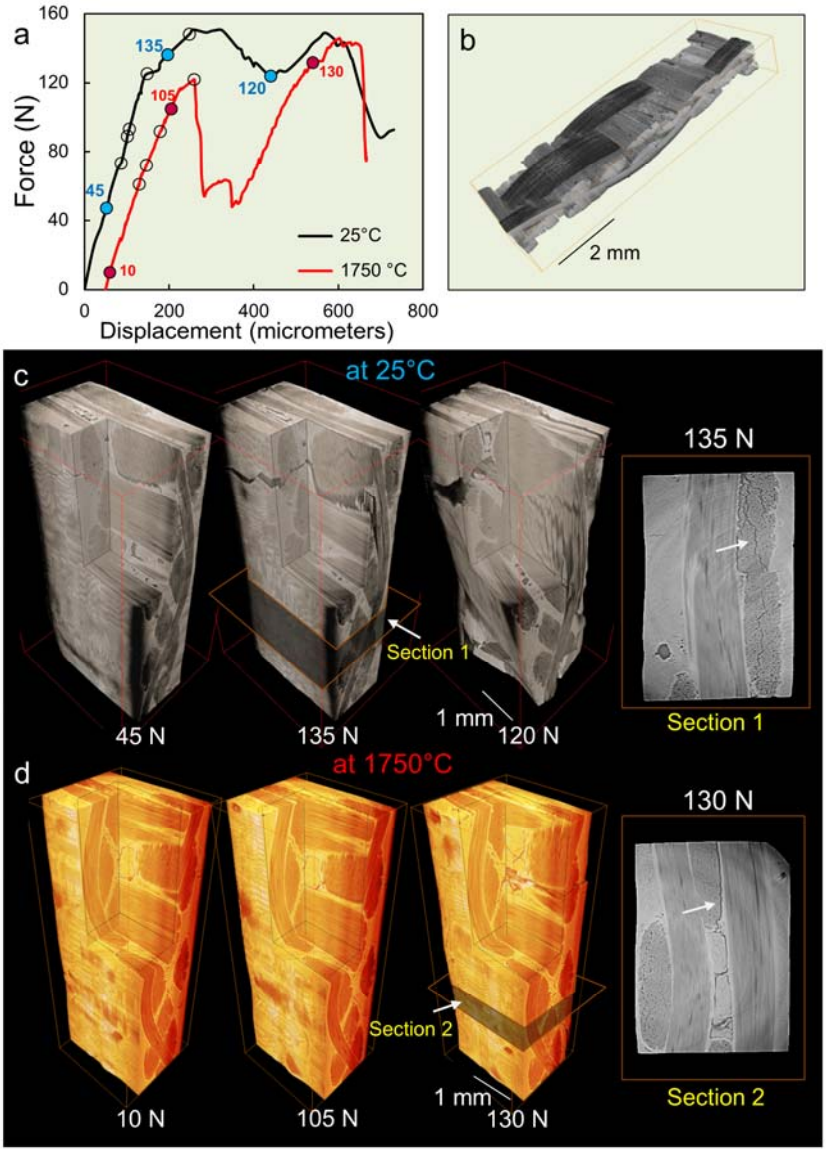

Figure 4. ***In situ*** **tomography of C-SiC composite with textile-based carbon fiber reinforcements under tensile load at 25°C and 1750°C. (a)** Force-displacement curves showing loads at which μ-CT data were collected. Red curve offset by 60 μm for visual clarity. Hollow circles indicate acquired μ-CT data at that load; blue and red solid circles indicate loads corresponding to images in (c) and (d) respectively. **(b)** μ-CT image from composite plate after partial infiltration of SiC matrix illustrates the architecture of the woven fiber tows within the test samples. (**c**) & (**d**) μ-CT images showing development of damage in specimens tested at room temperature (c) and at 1750°C (d). The higher magnification slices at the right, from sections 1 and 2, show different cracking mechanisms (indicated by arrows) in the later stages of failure: at room temperature, splitting cracks grow within the axial fiber tows; at high temperature, cracks grow along the boundary between the axial fiber tows and the matrix. Additionally, detailed animations of the complete sets of μ-CT data from these two tests are included in the videos S3 and S4 in the Supplementary online information.